# Design of a High Gain Yagi-Uda Antenna Array for VHF-Band Radar Applications

**Basim K. J. Al-Shammari**
Electrical Engineering Department, College of Engineering, Wasit University, Wasit, Al Kut, Iraq
bkhalaf@uowasit.edu.iq

**Ismail Sh. Hburi**
Electrical Engineering Department, College of Engineering, Wasit University, Wasit, Al Kut, Iraq
isharhan@uowasit.edu.iq

**Hala A. Naman**
Electrical Engineering Department, College of Engineering, Wasit University, Wasit, Al Kut, Iraq
haltaee@uowasit.edu.iq

**Haider Th. Salim Alrikabi**
Electrical Engineering Department, College of Engineering, Wasit University, Wasit, Al Kut, Iraq
hdhiyab@uowasit.edu.iq (corresponding author)

**Hasan F. Khazaal**
Electrical Engineering Department, College of Engineering, Wasit University, Wasit, Al Kut, Iraq
hfahad@uowasit.edu.iq

**Kdhim A. Neamha**
Ministry of Sciences and Technology, Iraq
kadhim@alnesagh.me

**Ahmed J. Qasim**
Ministry of Sciences and Technology, Iraq
Ahmedjafar23@yahoo.com

*Received: 3 August 2024 | Revised: 16 August 2024 | Accepted: 22 August 2024*

 *DOI: https://doi.org/10.48084/etasr.8607*

**ABSTRACT**

**The radar of the Yagi-Uda antenna array offers useful traits for the detection of stealth targets. It employs the Very High Frequency (VHF) band, which has the advantage of counteracting stealth technology, as the shape of the target and the absorbing materials used for absorbing radar signals are less efficient against VHF. Moreover, the meter wavelength enables the radar to detect targets at distances exceeding those accessible to millimeter- and centimeter-wave radars. Nevertheless, the range of detection of this type of radar remains constrained and requires further development. The majority of current research is concentrated on the signal processing aspect, with less focus being placed on the antenna array. The antenna elements represent a crucial component of the radar station. This article presents a novel development of the traditional 16-element Yagi-Uda antenna array, which is commonly used in surveillance radar systems operating at a meter frequency band. The development is achieved through a modification of the previously mentioned antenna, which aims to increase the directivity of the antenna array, with a minimum cost and the same signal processing as the original antenna array platform. An additional two-row Yagi-Uda antenna array is proposed, comprising 14 elements in each row and an associated power unit. This modification is designed to enhance the pattern characteristics of the array. Simulation and measurement results for the pattern of the antenna indicate that the achieved gain for the**

**proposed modification is more than 3 dB in compression compared to that of the traditional 16-element array.**

***Keywords-VHF band radar; Yagi-Uda antenna; antenna array; power divider unit; antenna radiation patterns***

## I. INTRODUCTION

The traditional 16-element Yagi-Uda antenna array radar is a two-dimensional antenna configuration that operates within the VHF range and is regarded as a metric system that employs a long wavelength. The technology was used by military forces for surveillance purposes, having employed it as an early warning radar to detect long-distance airborne targets. Accordingly, it is integrated with a surface-to-air missile system to create an integrated system, typically referred to as an air defense battery. The particular radar boasts a number of useful features for the detection of stealth targets operating within the VHF band. This range of frequencies is particularly effective in countering stealth technology, as the shape of the target and the absorbing materials used to deflect radar signals are less efficient against VHF [1-3]. Moreover, the meter wavelength endows the radar with the capacity to detect targets at distances exceeding those accessible to millimeter and centimeter-wave radars. This specific type of radar system was first deployed in 1970 [4-6], and remains operational today, with numerous corporations manufacturing and supplying modified versions to enhance reliability and efficiency, and replace obsolete components. Recently, enhancements have been made to the original 16-element system, and the entire system has been repackaged into a standard container and distributed in several tens of units [7, 8]. Authors in [9], present a VHF band Yagi antenna scheme for radar purposes. They design an array composed of two rows, each consisted of six elements. Each element is a Yagi-Uda antenna (single-folded dipole) optimized to run at 165 MHz. Through simulation, the authors observed that rotating the array beam with a 65-degree phase shift would not change the level of the azimuth side lobe.

Conversely, the level of the elevation side lobe will increase, while the directivity will decline to a slight degree. The majority of previous research has concentrated on the signal processing aspect, rather than on the antenna array itself. As the antenna elements are the fundamental component of the radar station, this paper primarily focuses on enhancing the antenna of the radar system. This is achieved by reducing the sidelobe level and increasing the gain and overall performance of the antenna. In contrast to the approach taken in [9], this study introduces a two-row Yagi-Uda antenna array, with each row consisting of 14 elements and an associated power distributor. This is intended to enhance the pattern characteristics of the antenna. Specifically, this article presents a power divider unit that ensures each element receives the requisite power within the system's total power budget, using a matched coaxial cable for each antenna. The document is organized firstly with a detailed description of the Yagi–Uda antenna design, followed by the experimental and analytical results for the proposed array configuration.

## II. ANTENNA ARRAY DESIGN DESCRIPTION

The initial step is to delineate the individual component of the VHF antenna array, specifically the Yagi-Uda antenna, and to provide supplementary information regarding the optimization of the antenna dimensions. Subsequently, the overall array characteristics of the traditional 16-element two-row Yagi-Uda antenna array will be discussed. A fundamental aspect of Yagi antenna theory is the understanding of the phases of currents flowing through the various components of the antenna [10-12]. The parasitic elements of the Yagi antenna function by assigning disparate phases to their signals in comparison to that of the driven component. In specific directions, the signal is enhanced while being diminished in others. As the supplementary antenna elements in the Yagi are not directly powered but rather harvest power from the primary element, these additional components are referred to as "parasitic" elements. One limitation of the Yagi antenna design is the absence of a direct power supply for the additional elements. Consequently, the phase and amplitude of the exciting current are not fully regulated. Its functionality is contingent upon the dipole, the length of the element, and the distance between elements. An element may be constructed in either an inductive or a capacitive manner in order to achieve the requisite phase shift. Each form of reactance exerts a discernible influence. In the inductive element, the induced currents are observed to be in a phase relationship that causes signal power to be reflected back from the parasitic element (reflector).

By adjusting the frequency below the resonance point, the element can be rendered inductive. This can be achieved by inserting a physical inductance (coil) that is longer than the powered element by approximately five percent. In contrast, the phase of induced currents in the case of a capacitive parasitic element exerts control over the direction of radiated power, directing it to the direction of the parasitic element (director). This can be accomplished by turning it above resonance or by adding some capacitance to the element, whereby the latter is made approximately 5 percent shorter than the former. The following example demonstrates the optimization of a 6-element Yagi-Uda antenna via surrogate global optimization for both the radiation patterns and the matching input impedance of the two antennas [13, 14]. The input impedance and directivity are susceptible to alteration by the parameters that describe the radiation patterns. The multidimensional surface on which such optimizations must be performed exhibits numerous local optima. This renders the identification of the optimal set of variables to achieve the desired optimization targets particularly challenging, as these targets are defined in terms of global optimization approaches [15]. Table I presents the set of parameters used in the antenna design, while the initial design values are selected at the center of the VHF band.

The fundamental operational principle of this Yagi-Uda antenna is the dipole. In the case of this particular antenna, this constitutes the standard exciter. The length of the dipole is selected to be approximately equal to the wavelength at the design frequency.

TABLE I. EXAMPLE OF YAGI ANTENNA PARAMETER SETTING

| Parameter | Setting |
|---|---|
| Center frequency | 144.5 MHz |
| Wire diameter | 12 mm |
| Wavelength | 2.076 m |
| Output impedance | 50 Ohm |
| Bandwidth | 2.16 MHz |
| Minimum frequency | 140.16 MHz |
| Maximum frequency | 148.83 MHz |

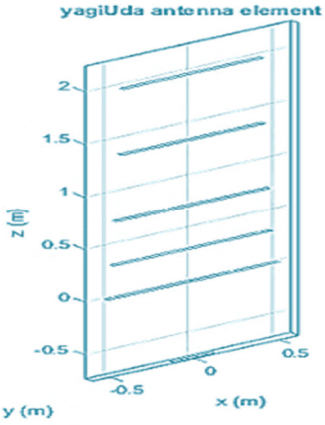


Fig. 1. The first design geometry of the antenna element.

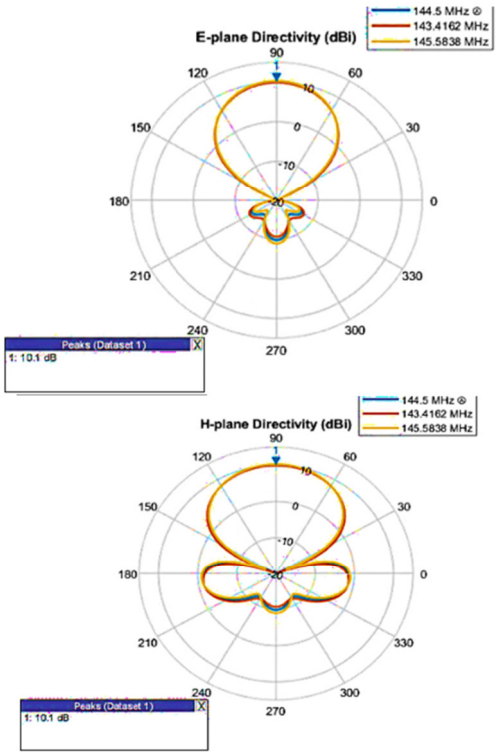


Fig. 2. The electric field in (a) H-planes and (b) E-planes.

The number of directors should be configured to be four and the initial hypothesis regarding the spacing between the elements and the element lengths will serve as a starting point for the optimization process. Figure 1 presents the initial design hypothesis [16]. Figure 2 provides a prediction of the radiation pattern for the initial design in a three-dimensional space prior to the implementation of the optimization process. The initial design exhibits inadequate directivity in the requisite orientation (90-degree elevation).

Figure 2 shows the respective electric field plot in the H and E planes (azimuth = 0 and 90 degrees, normalized magnitude). Figure 3 examines the Voltage Standing-Wave Ratio (VSWR) for the coaxial cable and the impedance of the Yagi antenna as the load at the frequencies for which the system is designed to operate.

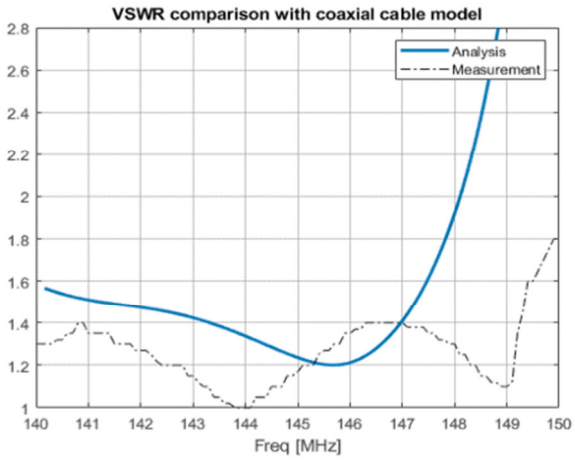


Fig. 3. The VSWR for the coaxial cable and the Yagi's impedance.

### *A. The 16-Element Yagi Antenna Array Specifications*

The 16-element scheme comprises an antenna array that is used for the transmission and reception of the signal on the VHF band. The array comprises 16 Yagi antennas, arranged in two rows of eight elements each. The antenna system is installed on the vehicle used for its conveyance, thereby enhancing mobility. Moreover, the array's mechanical attributes permit adjustments to its tilt and height through operational manipulation. The horizontal angle scanning is performed by the array via a mechanical rotational movement at a rate of 10 rpm. Three distinct indicators are employed for this purpose, including a backup A-scope and two plan location indicators [17-19]. The initial version of this radar included a coaxial cavity resonator transmitter, a transistor-based preamplifier, and a vacuum tube receiver with a vacuum tube/pin diode-based duplexer. The system was equipped with an automatic controller of four pre-set working frequencies and an indicator of moving targets, which served to eliminate jamming and passive clutter. Additionally, the system could be coupled with another radar to facilitate tracking on its display. The specifications of the antenna are presented in Table II. The transmitter of the radar apparatus transmits the power to the antenna via a divider. The power divider provides the requisite power to the two rows of the antenna with a phase shift of 90° between them, allocating 40% of the total power to the upper row and 60% of the total power to the lower row.

The power sources will be connected to the elements via coaxial cables. The analysis of a single element within the array revealed that the antenna was designed deploying the method of the surface wave. This is in order to provide compensation for the use of relatively large sections of radiators or dipoles, in case an antenna of the Yagi type has been employed. This is due to the fact that the wavelength in question is relatively long, at approximately 1.875 meters. Each element or antenna in the array has a short circuit at the far end of it, which is used to create an open circuit at the end of the line, thereby compensating for the use of the large Yagi antenna. This occurs because the length of the two wirelines is equal to $\lambda/4$. As the short circuit is situated at this distance, the characteristic impedance can be calculated as:

$Z_o = jtan\,\beta l$ where $is\ \frac{2\pi}{\lambda}$, therefore we have:

$Z_o = jtan\frac{2\pi}{\lambda}\frac{\lambda}{4}$ and $Z_o = \infty$.

Therefore, the presence of a short circuit at the end of the line renders this end an open circuit, thereby compensating for the use of a large antenna. The characteristic impedance is 75 Ω, while the radiation pattern is depicted in Figure 4, which presents the results of the measurement method for parameter setting as outlined in Table II.

TABLE II. THE RADAR ANTENNA SPECIFICATIONS [20]

| Item | Specifications | Item | Specifications |
|---|---|---|---|
| Frequency | VHF (160 MHz) | Maximum transmitting power | 400 W |
| Range | 250 km | Average transmitting power | 260 W |
| Altitude | 35 km | Array length | 15.4 m |
| Azimuth | 360 degrees | Array width (element length) | 2.1 m |
| Elevation | -5 into 15 degrees | Spacing between the two rows (center to center) | 2.45 m |
| Precision | 1 km range | Spacing between two elements (center to center) | 2.2 m |
| | | Half Power beam width | 6 degrees |

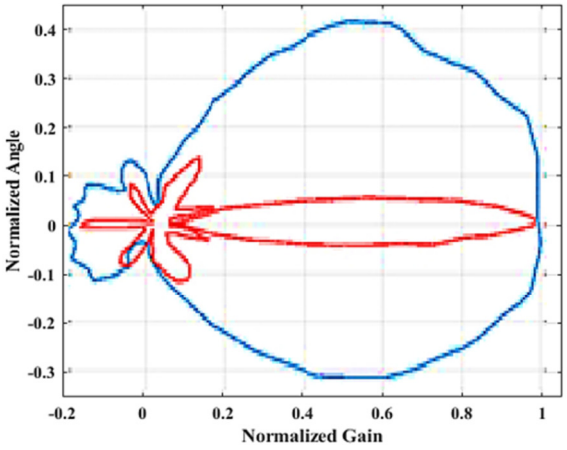


Fig. 4. Horizontal field pattern, the blue curve is for the one element Yagi antenna, and the red curve is for the 16-element Yagi array.

Furthermore, Figure 5 presents the vertical radiation patterns of antennas at $h_{up}$ = 6.35 m and $h_{low}$ = 3.9 m, with field phases of (0° and 180°) in the upper-tier lobe and field phases of (90° and 270°) in the lower-tier lobe.

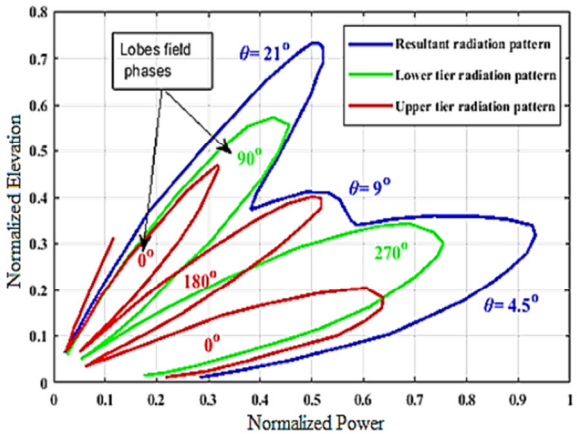


Fig. 5. The theoretical radiation pattern of the original array antenna at different elevation angles.

## B. Power Divider Unit

The power distribution unit plays a significant role in the performance of the antenna. As shown in Figure 6, the unit comprises strip lines with a single input and four output ports, with two output ports for each row of antennas. The unit exhibits an input and an output impedance of 75 Ω. In order to evaluate the functionality of the power divider unit, the performance characteristics illustrated in Figures 6 and 7 must be first examined.

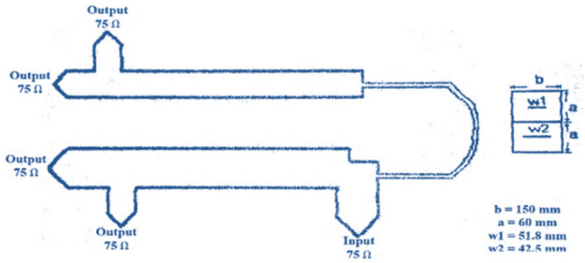


Fig. 6. Power divider unit.

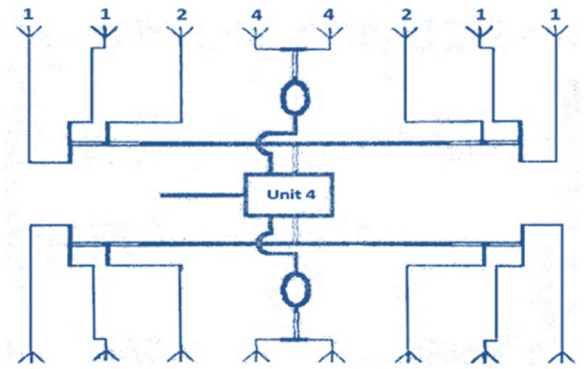


Fig. 7. Antenna array with the power divider unit.

The input impedance is 75 Ω, and the unit will allocate the power for the signal at a rate of 40% for the upper row $P_1$ and 60% for the lower row $P_2$, as:

$$P_1 = (I\frac{R_2}{R_1+R_2})^2.R_1 \quad (1)$$

$$P_2 = (I\frac{R_1}{R_1+R_2})^2.R_2 \quad (2)$$

$\frac{P_2}{P_1} = \frac{0.6}{0.4} \; then \Longrightarrow \frac{0.6}{0.4} = \frac{R_1}{R_2}$, which yields,

$$R_1 = 1.5\,R_2, \quad (3)$$

$$\frac{R_1.R_2}{R_1+R_2} = 75\ \Omega \quad (4)$$

From (3) and (4), it can be ascertained that $R_1$ = 125 Ω and $R_2$= 187.5 Ω. Figure 8 determines the characteristic impedance of the strip lines. Additionally, there is a narrow strip line equal to $\lambda/4$, which exhibits a phase difference of 90° between the upper and lower rows.

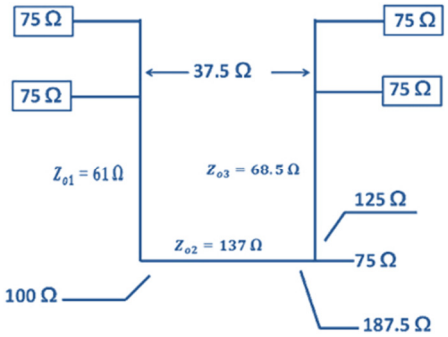


Fig. 8. Impedance designation of the power distribution unit.

### C. Power Distribution for the Antenna Elements

As displayed in Figure 7, the power is distributed among the constituent elements of the antenna array. The use of coaxial cables with a characteristic impedance of 75 Ω is employed. The phase difference between the elements of a given row is zero, provided that the connection cables are of the same length from the power divider to each element. The matching between the elements of the array and cables can be achieved through the use of an impedance transformer, which is essentially a coaxial cable of 33 cm in length. This transformer is utilized for the purpose of transforming the impedance from 37.5 Ω to 75 Ω and vice versa. The transformer's characteristic impedance can be calculated as: $Z_o = \sqrt{75 \times 37.5} \approx 53\,\Omega$. This specific type of impedance transformer is typically constructed with a length of $\lambda/4$. However, for design considerations, the designer may use an inner insulator which is the insulator between the inner and outer conductor of the coaxial cable, as shown in Figure 9, with a high dielectric constant to reduce the length of the cables. In this particular configuration, the transformer behaves as an impedance transformer.

In order to prove this, the following stages must be implemented:

$$Z_o = \frac{138}{\sqrt{\varepsilon_r}} log_{10}\left(\frac{D}{d}\right) \quad (5)$$

If we consider $= \frac{\omega}{v_o}$, and $v_o = \frac{c}{\sqrt{\mu_r \varepsilon_r}}$, we have, $\beta = \frac{2\pi f_o}{c}\sqrt{\mu_r \varepsilon_r}$ and for $\mu_r = 1$, yields $\beta = \frac{2\pi}{\lambda_o}\sqrt{\varepsilon_r}$. Now, to obtain a phase shift of 90° $= \frac{\pi}{2}$ we employ $\beta l = \frac{\pi}{2} = \frac{2\pi}{\lambda_o}\sqrt{\varepsilon_r}\,L$, where, $L = \frac{\lambda_o}{4\sqrt{\varepsilon_r}}$, $\lambda_o$ =1.875 m, $l$ = 33 cm, $\varepsilon_r$ =1.91, d = 4.7 mm, and D = 15.4 mm. Substitution of these parameters into (5) gives $Z_o = \frac{138}{\sqrt{1.91}} log_{10}\left(\frac{15.4}{4.7}\right) \approx 51.4\,\Omega$. Figure 7 demonstrates that the supplied power to elements 1, 2, 7, and 8, commencing from the left or right side of the upper or lower row of the antenna, is equivalent to one sixteenth of the supplied power to each row. In contrast, the supplied power is doubled to elements 3 and 6, and this power is then doubled again when supplied to elements 4 and 5. The supplied power to each row will be distributed between the elements of the row, as presented in Table III. For the sake of simplicity, the notation 1124 4211 is employed to represent this power distribution policy.

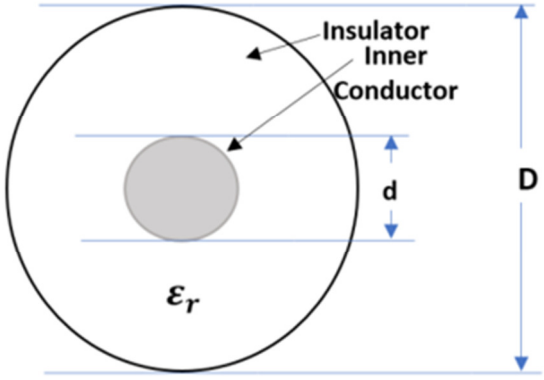


Fig. 9. The coaxial cable profile.

TABLE III. THE POWER DISTRIBUTION FOR THE UPPER AND LOWER ELEMENTS

| Element No. | 1 | 2 | 3 | 4 | 5 | 6 | 7 | 8 |
|---|---|---|---|---|---|---|---|---|
| Supplied power of each element in the two rows | 6.25% | 6.25% | 12.5% | 25% | 25% | 12.5% | 6.25% | 6.25% |
| Notation | 1 | 1 | 2 | 4 | 4 | 2 | 1 | 1 |

As previously stated, the range of operating frequencies renders the 16-element radar system an optimal tool for combating hidden targets. However, authors in [6] deployed the Radar Cross Section (RCS) metric to examine the impact of using absorption materials as a stealth technology for finite cylindrical targets. The RCS ($\sigma$) for the target, as authors in [6, 20] consider is:

$$\sigma = 4\,\pi\,R^2\,\frac{|\vec{\Xi}_S|^2}{|\vec{\Xi}_t|^2} \quad (6)$$

where $R$ is the distance to the target, $\Xi_t$ is the field falling on the target, and $\Xi_S$ is the field scattered by the cylindrical target. Figure 10 presents the RCS of a cylinder with a length of 1 m and a radius of 6 mm. The RCS of a cylinder coated with a perfect absorption material, as predicted by the Macdonald model, is represented by the bold line. The RCS of a perfectly conducting cylinder is represented by the thin line.

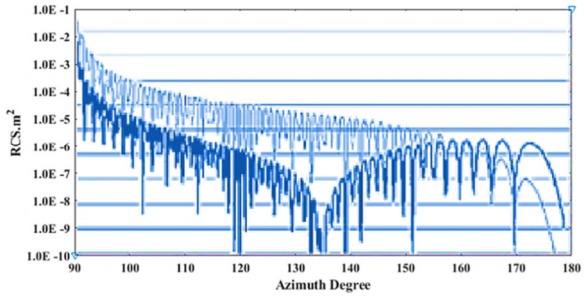


Fig. 10. Radar Cross Section (RCS) of a cylindrical volume [6].

### *D. Proposed Yagi-Uda Antenna Array*

As noted previously, the system was operational in 1970. Despite its obsolescence, the radar has undergone several modifications that have enabled its continued operation and significantly enhanced its original capabilities. The modified array is capable of automatically monitoring and collecting information signals from sensors of other radars. The signal can be conveyed in an accepted format via a multitude of communication channels. The radar provides additional features, including built-in test equipment, a minimum cost, a simplified adjustment procedure, a modular solid-state stable transmitter, fail-soft, and the maximization of Commercial Off-The-Shelf (COTS) components [21, 22]. The receiver employs a remote radar control with an optical cable over distances of between 100 and 500 meters. Additionally, authors in [23, 24] describe an upgrade to a long-range VHF (ground-based) monitoring radar that provides robust pulse interference protection and resilience against active jamming. The level of jamming is continuously and graphically displayed to the operators. The safety of the signal is ensured by extending the signal processor's dynamic range and electronic frequency agility capability. By deploying the digital adaptive Moving Target Indicator (MTI) and clutter map generation, passive interference is effectively rejected. Table IV exhibits the key features of this version.

### *E. Design and Implementation of the Proposed Antenna Array*

The original antenna was analyzed, and a new design was proposed to enhance its gain and performance, hence improving the overall performance of the radar. In this study's proposal, the number of elements in each row of the station is increased by six, resulting in a total of 28 elements, as shown in Figure 11. The antenna is considered a linear array type. In order to ascertain the resultant field pattern of the antenna in the horizontal plane, i.e., the azimuth pattern, it is necessary to characterize the field pattern of one element as well as the array factor of the array.

Equation (7) presents the methodology for calculating the resultant field pattern of an array antenna:

$$E_R = F_1 . F_2 \quad (7)$$

where $E_R$ is the resultant field pattern, $F_1$ is the field pattern of a single element, and $F_2$ is the array factor. The field pattern of the element is described as:

$$F_1 = f(\theta) = |\cos(\theta)|^k \quad for\ k = 1,2,3,..,n \quad (8)$$

In order to select the appropriate value of $k$, it is necessary to employ a curve-fitting approach for the practical values portrayed in Table IV and the theoretical values of the field pattern for varying values of $k$. If each element of the array is considered to act as a point source, then the array equation is given by:

$$F_2 = \sum_{n=1}^{N-1} A_n e^{j\psi} \quad (9)$$

where $A_n$ is the amplitude of the field, $N$ is the number of elements, and $\psi = \beta d \cos(\theta)$ is the phase shift angle. The elevation pattern of the antenna is contingent upon the power distribution of the elements, the distance between the two rows of the antenna, and the height of the antenna from the ground plane. The elevation pattern depicted in this figure was obtained from the technical specifications manual and represents the original pattern at varying angles and heights relative to the ground plane.

TABLE IV. SOME FEATURES OF THE IMPROVED LONG-RANGE VHF VERSION

| **Specification** | **Value** | |
|---|---|---|
| | After upgrading | Before upgrading |
| Frequencies' Range | 140-180 MHz | 150-170 MHz |
| Steps of frequencies | 200.0 kHz | Four discrete frequencies |
| Accuracy of frequency setting | ±10.0 kHz | |
| Pulse power for the $T_x$ | 8.0 kW | 300.0 kW |
| Structure changes and signal Power instant probing | applied | Not applied |
| Probing-pulse | | |
| Short pulse | 6.0 µs | 6.0 µs |
| PSK- signals: | | |
| 42-bit | 42× (6.0 µs) | |
| 13-bit | 13× (6.0 µs) | |
| Accuracy of detection | | |
| Range | 0.18 km | 1.4 Km |
| Azimuth | 0.4° | 1.5° |
| Time for start-up | 3.0 min | 8.0 min |
| Consumption of Power | up to 6.0 kW | 10.0 kW |

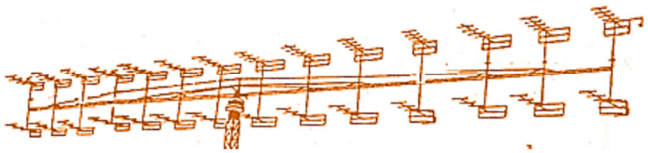

Fig. 11. Sketch of the proposed antenna array.

It is essential that the power supplied to the developed antenna be distributed between its elements in a manner that does not affect the main beam width of the resultant field and the number and strength of the sidelobes of the resultant field. The gain of the antenna must also be considered. In order to satisfy these requirements, a novel power divider comprising 28 ports has been devised and deployed, as illustrated in Figure 12. The power fraction for each element is specified in Table V. The station has been subjected to experimental testing with the recently designed antenna, comprising 28 elements arranged in two rows of 14 elements each. This antenna has been installed on the radar truck, as shown in Figure 11. The

experimental results of the new system demonstrate a narrow main beam width and a low sidelobe level. Table VI presents the parameters used in the experiment and the resulting data. Moreover, the rotation of the novel antenna was evaluated at varying speeds (2, 4, and 6 rpm) to ascertain the structural stability and the resilience of the rotating joints to the additional mass of the antenna during operation.

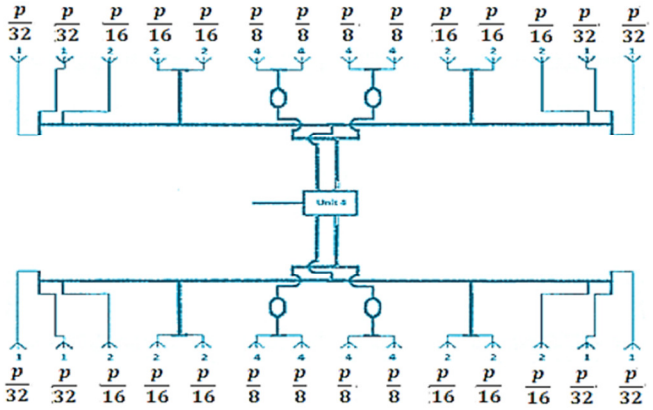


Fig. 12. Power divider unit for the proposed version.

TABLE V. THE POWER DISTRIBUTION FOR THE ELEMENTS OF THE MODIFIED VERSION

| **No.** | **1** | **2** | **3** | **4** | **5** | **6** | **7** | **8** | **9** | **10** | **11** | **12** |
|---|---|---|---|---|---|---|---|---|---|---|---|---|
| Power | *p*/32 | *p*/32 | *p*/16 | *p*/16 | *p*/16 | *p*/8 | *p*/8 | *p*/16 | *p*/16 | *p*/16 | *p*/32 | *p*/32 |
| Percentage (%) | 3.125 | 3.125 | 6.25 | 6.25 | 6.25 | 12.5 | 12.5 | 6.25 | 6.25 | 6.25 | 3.125 | 3.125 |
| Notation | 1 | 1 | 2 | 2 | 2 | 4 | 4 | 2 | 2 | 2 | 1 | 1 |

TABLE VI. SOME FEATURES OF THE MODIFIED P-18 VERSION

| **Parameter** | **Value** | |
|---|---|---|
| | Before modification | After modification |
| No. of elements per a row | 8 | 14 |
| Center frequency | 160 MHz | 165 MHz |
| Distance between elements | 2.2 m | 2.2 m |
| Element half power beam width | 50.942 deg. | |
| Array half power beam width $\theta_{-3dB}$ | 6.287 deg. | 3.5 deg. |
| Directivity $G$ | 23.04 dB | 26.8 dB |
| Length of array | 15.4 m | |
| Notations for fraction of power distribution | 11244211 | 11222444422211 |

## III. A PRACTICAL TEST OF THE DEVELOPED SYSTEM

In order to test the developed system in a practical setting, a transmitter of a low power level was installed at a distance of 1,000 meters from the radar under examination. The system is operated and connected to the radar so as to measure and record the radiation pattern of the original and new antenna using the pre-installed display for radiation pattern recording. The test is conducted in the operational field, taking into account all relevant contextual factors. Figure 13 illustrates the radiation pattern of the original and developed antennas, namely the directivity characteristics of the proposed antenna array transmitting and receiving the requisite signal. Figure 14 portrays the theoretical results, the antenna dimensions, and the radiation's main beam of the width (-3 dB beam-width) of 3.5 degrees. In this regard, beam width represents the angular dispersion of the electromagnetic radiation emitted from the antenna array, expressed in vertical and horizontal degrees. The results demonstrate that the modified antenna exhibits a narrower beam width than that of the original antenna, indicating a higher degree of directivity. The achieved gain is in excess of 3 dB in comparison to that of the traditional 16-element arrays. Nevertheless, these advantages are accompanied by certain drawbacks in terms of design complexity and array dimensions, which require further investigation to be effectively addressed.

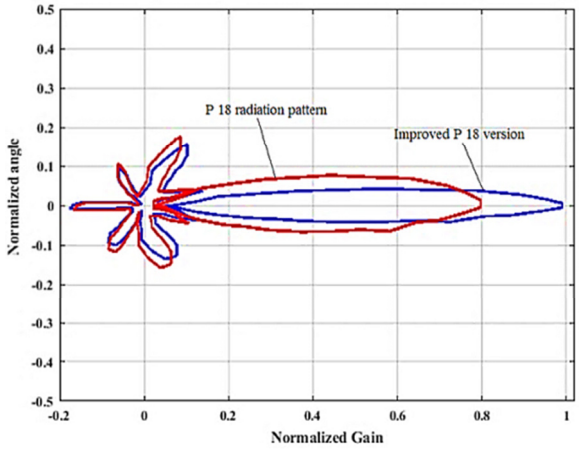


Fig. 13. Curve fitting between theoretical and practical field pattern at different values of $k$ factor.

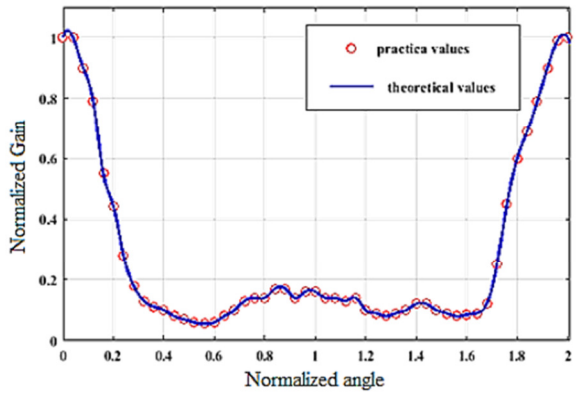


Fig. 14. Simulation results for the radiation pattern of the original and modified array antenna at different elevation angles.

## IV. CONCLUSIONS

Given the critical role of the antenna elements in radar systems, this paper proposes a 16-element Yagi-Uda array for use in VHF band radar applications, offering high gain and antenna directivity. This type of antenna is particularly well-suited for the detection of stealth targets. The operating range of frequencies allows for the contrasting of stealth technology, whereby the shape of the target and the absorbing materials used for absorbing radar signals are less efficient against VHF.

Moreover, the meter wavelength enables the radar to detect targets at distances exceeding those accessible to millimeter and centimeter-wave radars. This paper presents the development of traditional 16-element Yagi-Uda antenna arrays used by surveillance radar in a meter frequency band. The expansion is achieved through a modification of the previously described antenna, which increases the antenna array directivity while maintaining a minimum cost and the same signal processing as the original antenna array platform. An additional two-row Yagi-Uda antenna array is also included, with each row consisting of 14 elements and an associated power unit, which serves to further enhance the pattern characteristics of the array. Simulation and measurement results for the antenna pattern indicate that the proposed modification achieves a gain of more than 3 dB in compression compared to that of the traditional 16-element array. Further investigation could be conducted regarding the current work, for example, the proposed structure could be supported with further development of the digital signal processing to improve the directivity and the detection of the system.

## REFERENCES


[1] J. Röttger, "Reflection and scattering of VHF radar signals from atmospheric refractivity structures," *Radio Science*, vol. 15, no. 2, pp. 259–276, 1980, https://doi.org/10.1029/RS015i002p00259.

[2] H. Kuschel, "VHF/UHF radar. Part 1: Characteristics," *Electronics & Communication Engineering Journal*, vol. 14, no. 2, pp. 61–72, Apr. 2002, https://doi.org/10.1049/ecej:20020203.

[3] C. Bianchi, U. Sciacca, A. Zirizzotti, E. Zuccheretti, and J. A. Baskaradas, "Signal processing techniques for phase-coded HF-VHF radars," *Annals of Geophysics*, vol. 46, no. 4, pp. 697–705, Dec. 2003, https://doi.org/10.4401/ag-4369.

[4] G. Sato, "A secret story about the Yagi antenna," *IEEE Antennas and Propagation Magazine*, vol. 33, no. 3, pp. 7–18, Jun. 1991, https://doi.org/10.1109/74.88216.

[5] V. S. Chernyak and I. Y. Immoreev, "A Brief History of Radar," *IEEE Aerospace and Electronic Systems Magazine*, vol. 24, no. 9, pp. B1–B32, Sep. 2009, https://doi.org/10.1109/MAES.2009.5282288.

[6] O. Sukharevsky, Ya. Belevshchuk, V. Vasilets, and S. Nechitaylo, "Radar cross-section calculation method for antenna of P-18 radar station," in *2010 International Conference on Mathematical Methods in Electromagnetic Theory*, Kyiv, Ukraine, Sep. 2010, pp. 1–4, https://doi.org/10.1109/MMET.2010.5611345.

[7] J. Pejřil, "Simulace vysílání radiolokátoru pomocí softwarově definovaného rádia," BSc Thesis, Univerzita Pardubice, Pardubice, Česká Republika, 2021.

[8] A. Belous, "Methods and Means of Ensuring Reliability of Radar and Communication Systems," in *Handbook of Microwave and Radar Engineering*, 1st ed., A. Belous, Ed. Cham, Switzerland: Springer International Publishing, 2021, pp. 661–775.

[9] H. Mubarak and M. Makkawi, "Design, Simulation and Performance Analysis of Yagi Antenna Array For VHF Radar," in *2018 International Conference on Computer, Control, Electrical, and Electronics Engineering (ICCCEEE)*, Khartoum, Sudan, Aug. 2018, pp. 1–5, https://doi.org/10.1109/ICCCEEE.2018.8515780.

[10] R. Kullock, M. Ochs, P. Grimm, M. Emmerling, and B. Hecht, "Electrically-driven Yagi-Uda antennas for light," *Nature Communications*, vol. 11, no. 1, Jan. 2020, Art. no. 115, https://doi.org/10.1038/s41467-019-14011-6.

[11] G. Thiele, "Analysis of yagi-uda-type antennas," *IEEE Transactions on Antennas and Propagation*, vol. 17, no. 1, pp. 24–31, Jan. 1969, https://doi.org/10.1109/TAP.1969.1139356.

[12] H. R. Katireddy, M. V. Narayana, and G. Immadi, "Innovative Design and Analysis of an Electrically Small Reconfigurable Antenna for GPS and Blue Tooth Applications," *Engineering, Technology & Applied Science Research*, vol. 11, no. 5, pp. 7684–7688, Oct. 2021, https://doi.org/10.48084/etasr.4465.

[13] Z. M. F. Ferran, L. A. T. Ongquit, E. R. Arboleda, Z. M. F. Ferran, L. A. T. Ongquit, and E. R. Arboleda, "Review on trends and recent development on Yagi-Uda antenna designs for 5G communication applications," *International Journal of Science and Research Archive*, vol. 12, no. 2, pp. 391–407, 2024, https://doi.org/10.30574/ijsra.2024.12.2.1242.

[14] S. Koziel and A. Bekasiewicz, *Multi-Objective Design of Antennas Using Surrogate Models*. New Jersey, USA: Wspc, 2016.

[15] H. T. S. Alrikabi, I. A. Aljazaery, and A. H. M. Alaidi, "Using a Chaotic Digital System to Generate Random Numbers for Secure Communication on 5G Networks," *Engineering, Technology & Applied Science Research*, vol. 14, no. 2, pp. 13598–13603, Apr. 2024, https://doi.org/10.48084/etasr.6938.

[16] A. Papathanasopoulos, P. A. Apostolopoulos, and Y. Rahmat-Samii, "Optimization Assisted by Neural Network-Based Machine Learning in Electromagnetic Applications," *IEEE Transactions on Antennas and Propagation*, vol. 72, no. 1, pp. 160–173, Jan. 2024, https://doi.org/10.1109/TAP.2023.3269883.

[17] R. Malinauskas, *Aviacinės radiolokacinės sistemos*. Vilnius, Lithuania: Vilnius Gediminas Technical University, 2007.

[18] I. J. Busch-Vishniac, *Electromechanical Sensors and Actuators*. New York, NY, USA: Springer, 1999.

[19] M. Nahas, "A High-Gain Dual-Band Slotted Microstrip Patch Antenna For 5G Cellular Mobile Phones," *Engineering, Technology & Applied Science Research*, vol. 14, no. 3, pp. 14504–14508, Jun. 2024, https://doi.org/10.48084/etasr.7410.

[20] P. Y. Ufimtsev, *Fundamentals of the Physical Theory of Diffraction*, 2nd ed. Piscataway, NJ, USA: Wiley-IEEE Press, 2014.

[21] C. Kopp, "Russian / PLA Low Band Surveillance Radar Systems (Counter Low Observable Technology Radars)," Air Power Australia, APA-TR-2007-0901, Sep. 2007.

[22] C. Kopp, "Flanker Radars in Beyond Visual Range Air Combat," Air Power Australia, APA-TR-2008-0401, Apr. 2008.

[23] L. Zakhar'ev and A. Lemanskii, "Wave Scattering by "Black" Bodies," *Sovetskoe Radio, Moscow,* 1972.

[24] A. H. Alaidi, S. D. Chen, and Y. W. Leong, "Artificial Bee Colony with Crossover Operations for Discrete Problems," *Engineering, Technology & Applied Science Research*, vol. 12, no. 6, pp. 9510–9514, Dec. 2022, https://doi.org/10.48084/etasr.5250.